11-1-2011

Spectral phonon conduction and dominant scattering pathways in graphene

Dhruv Singh
Purdue University, singh36@purdue.edu

Jayathi Murthy
Purdue University, jmurthy@purdue.edu

Timothy Fisher
Purdue University, tsfisher@purdue.edu

Singh, Dhruv; Murthy, Jayathi; and Fisher, Timothy, "Spectral phonon conduction and dominant scattering pathways in graphene" (2011). *Birck and NCN Publications.* Paper 834.
http://dx.doi.org/10.1063/1.3656451

AIP | Journal of Applied Physics

Spectral phonon conduction and dominant scattering pathways in graphene

Dhruv Singh, Jayathi Y. Murthy, and Timothy S. Fisher

Citation: J. Appl. Phys. **110**, 094312 (2011); doi: 10.1063/1.3656451
View online: http://dx.doi.org/10.1063/1.3656451
View Table of Contents: http://jap.aip.org/resource/1/JAPIAU/v110/i9
Published by the American Institute of Physics.

Spectral phonon conduction and dominant scattering pathways in graphene

Dhruv Singh, Jayathi Y. Murthy,[a] and Timothy S. Fisher
School of Mechanical Engineering and Birck Nanotechnology Center, Purdue University, West Lafayette, Indiana 47906, USA

(Received 2 August 2011; accepted 16 September 2011; published online 9 November 2011)

In this paper, we examine the lattice thermal conductivity and dominant phonon scattering mechanisms of graphene. The interatomic interactions are modeled using the Tersoff interatomic potential and perturbation theory is applied to calculate the transition probabilities for three-phonon scattering. The matrix elements of the perturbing Hamiltonian are calculated using the anharmonic interatomic force constants obtained from the interatomic potential as well. The linearized Boltzmann transport equation is applied to compute the thermal conductivity of graphene for a wide range of parameters giving spectral and polarization-resolved information. The complete spectral detail of selection rules, important phonon scattering pathways, and phonon relaxation times in graphene are provided. We also highlight the specific scattering processes that are important in Raman spectroscopy-based measurements of graphene thermal conductivity, and provide a plausible explanation for the observed dependence on laser spot size. © *2011 American Institute of Physics*. [doi:10.1063/1.3656451]

I. INTRODUCTION

The thermal conductivity of graphite (in the basal plane) and diamond at room temperatures are close to 2000 W/m/K, higher than all other bulk solid crystals, making them excellent materials for thermal management. Measurements of the thermal conductivity of single and multiwalled carbon nanotubes have shown room temperature thermal conductivity greater than 3000 W/m/K[1,2] and are believed to result from one-dimensional phonon transport with low intrinsic scattering. The thermal conductivity of graphene was recently measured by Balandin *et al.*[3] to lie in the range of 3000–5000 W/m/K, indicating that single-layer graphene may have better thermal conduction properties than one-dimensional carbon nanotubes (CNTs). Since then, several other thermal conductivity measurements on single-layer, few-layer suspended[4–7] and substrate-supported[8–10] graphene have emerged. The results consistently indicate that the thermal conductivity of graphene is higher than graphite and diamond, and falls in the same range as CNTs.

Thermal conductivity measurements of several micron-sized suspended graphene flakes by micro Raman spectroscopy have recently appeared.[3–7] The energy transfer process involves photon-electron-phonon coupling, and published results appear to reveal a strong dependence on laser spot size. The thermal conductivity computed from these measurements is a result of the fact that power absorption primarily leads to generation of longitudinal phonons (through Normal electron-phonon scattering processes) a process whose time scale is 1 ps or less.[11] The measured thermal conductivity will therefore depend on the region over which the energy transfer from these modes to ZA modes can occur (since the ZA modes almost exclusively dominate heat conduction). It will also reflect a competition between the rate at which LA/LO phonon generation occurs and the rate at which these LA/LO phonons can scatter to ZA phonons. While an exact quantitative account of this mechanism can be given only by a direct simulation of the underlying processes, we believe that details of phonon scattering presented in this paper can enable simple estimates in device simulations and in interpreting thermal conductivity measurements. These details have not been outlined in any previous studies. The primary intent of this work is therefore to present a detailed understanding of phonon scattering processes and temperature-dependent phonon relaxation times in graphene, and to clearly elucidate their spectral dependence. The results presented complement recent experimental measurements, highlighting scattering mechanisms that are particularly important for Raman spectroscopy-based thermal conductivity measurements. Possible phonon scattering bottlenecks in graphene electronics and during optical absorption are also discussed.

A few groups have investigated phonon scattering and thermal conductivity in single- and few-layer graphene accounting for anharmonicity[5,12,13] using the Gruneisen constants determined from density functional theory (DFT). However all these studies have retained approximations similar to those of Klemens[14–16] for three-phonon scattering rates without considering phonon selection rules. Here we develop a methodology to obtain phonon spectra and thermodynamic and thermal transport properties of graphene using force fields from the Tersoff interatomic potential[17] with the parameterization of Lindsay and Broido.[18] Graphene thermal conductivity is computed using a solution of the linearized Boltzmann transport equation (BTE) in conjunction with perturbation theory.[19–23] While the general conclusions about thermal conductivity trends are similar to those reported recently,[24] we use a solution of the linearized BTE to understand the shift in the phonon distribution due to temperature gradients, the strong departure from the single mode relaxation time approximation indicated by our computations, and its effect on thermal conduction.

[a]Electronic mail: jmurthy@ecn.purdue.edu.

An alternative methodology to probe phonon transport is the use of molecular dynamics simulations which has been widely applied for thermal conductivity predictions of CNTs.[25–29] The computational complexity of MD simulations has usually restricted these simulations to small tube lengths, and compromises the computation of intrinsic thermal conductivity. Furthermore, MD simulations are classical and therefore do not accurately predict room- temperature relaxation times for graphene/CNTs because of their high Debye temperatures (>2000 K). Meanwhile, several molecular dynamics simulations of thermal transport in graphene nanoribbons have also recently appeared.[30–33] A discussion of these is presented toward the end of this paper.

II. PHONON-PHONON SCATTERING AND THERMAL CONDUCTIVITY

In computing thermal conductivity we follow the usual procedure of solving the Peierls- Boltzmann equation under weak nonequilibrium conditions (i.e., under a small temperature gradient). In principle, the BTE couples the population of each phonon mode $\vec{k}(p)$ (with wavevector $\vec{k}$ and polarization p) to all other interacting modes $\vec{k}'(p')$ and $\vec{k}''(p'')$. However, by a linearization of the BTE[19,21–23] and the definition of transition probability,[34,35] the phonon BTE can be transformed to an equation for the deviation of phonon population from equilibrium, $\vec{\Psi}_{\vec{k}(p)}$ (see supplementary materials)[35] which is independent of the temperature gradient ∇T and the actual occupation number of the other modes (at least directly) but depends only on their deviation from equilibrium as,

$$\vec{\Psi}_{\vec{k}(p)} = \frac{\hbar\omega_{\vec{k}(p)} n^0_{\vec{k}(p)}\left(n^0_{\vec{k}(p)}+1\right)}{\Gamma_{\vec{k}(p)} T}\vec{v}_{\vec{k}(p)} + \frac{A}{2\pi\hbar^2\Gamma_{\vec{k}(p)}} \times \left\{ \sum_{p',p''} \int n^0_{\vec{k}(p)} n^0_{\vec{k}'(p')}\left(n^0_{\vec{k}'(p')}+1\right)\left(\vec{\Psi}_{\vec{k}''(p'')} - \vec{\Psi}_{\vec{k}'(p')}\right) \left| \times \Im_{\vec{k}(p)+\vec{k}'(p')\leftrightarrow\vec{k}''(p'')} \right|^2 \frac{dk'_l}{|\vec{v}'_n|} + \frac{1}{2}\sum_{p',p''} \int n^0_{\vec{k}(p)}\left(n^0_{\vec{k}'(p')}+1\right) \times \left(n^0_{\vec{k}''(p'')}+1\right)\left(\vec{\Psi}_{\vec{k}''(p'')} + \vec{\Psi}_{\vec{k}'(p')}\right) \left| \Im_{\vec{k}(p)\leftrightarrow\vec{k}'(p')+\vec{k}''(p'')} \right|^2 \frac{dk'_l}{|\vec{v}'_n|} \right\} \Rightarrow \mathrm{M}\vec{\Psi}_{\vec{k}(p)} = \vec{\Psi}^0_{\vec{k}(p)}. \quad (1)$$

The first term on the right side is typically denoted as $\vec{\Psi}^0_{\vec{k}(p)}$ and depends only on the equilibrium occupation number of the interacting phonon modes through the quantity $\Gamma_{\vec{k}(p)}$,

$$\Gamma_{\vec{k}(p)} = \frac{n^0_{\vec{k}(p)}\left(n^0_{\vec{k}(p)}+1\right)}{\tau_{B,\vec{k}(p)}} + \frac{A}{2\pi\hbar^2} \times \left\{ \sum_{p',p''} \int n^0_{\vec{k}(p)} n^0_{\vec{k}'(p')} \times \left(n^0_{\vec{k}''(p'')}+1\right) \left| \Im_{\vec{k}(p)+\vec{k}'(p')\leftrightarrow\vec{k}''(p'')} \right|^2 \frac{dk'_l}{|\vec{v}'_n|} + \frac{1}{2}\sum_{p',p''} \int n^0_{\vec{k}(p)} \times \left(n^0_{\vec{k}'(p')}+1\right)\left(n^0_{\vec{k}''(p'')}+1\right) \left| \Im_{\vec{k}(p)\leftrightarrow\vec{k}'(p')+\vec{k}''(p'')} \right|^2 \frac{dk'_l}{|\vec{v}'_n|} \right\}. \quad (2)$$

In the above equations, $n^0_{\vec{k}(p)}$ represents the equilibrium occupation (Bose-Einstein distribution) of the phonon mode $\vec{k}(p)$, $\omega_{\vec{k}(p)}$ is its frequency, $\tau_{B,\vec{k}(p)}$ is the relaxation time due to boundary scattering and $\Gamma_{\vec{k}(p)}$ is its net scattering amplitude. A is the area of the Wigner-Seitz unit cell of graphene, T is the temperature, and $\hbar$ is reduced Planck's constant. Here the integrals are performed along k'_l, the line segment corresponding to $\omega + \omega'(p') - \omega''(p'') = 0$ (type 1 processes) with $\vec{v}'_n = \nabla_{\mathbf{k}''}\omega_{\mathbf{k}''p''} - \nabla_{\mathbf{k}'}\omega_{\mathbf{k}'p'}$[34,35] and $\omega + \omega'(p') - \omega''(p'') = 0$ (type 2 processes) with $\vec{v}'_n = \nabla_{\mathbf{k}''}\omega_{\mathbf{k}''p''} - \nabla_{\mathbf{k}'}\omega_{\mathbf{k}'p'}$. $\Im_{\vec{k}(p)+\vec{k}'(p')\leftrightarrow\vec{k}''(p'')}$ is the matrix element corresponding to the three phonon scattering event involving phonons $\vec{k}(p), \vec{k}'(p')$, and $\vec{k}''(p'')$. It contains terms from the third order derivatives $\phi^{l(0)m(i)n(j)}_{\alpha\beta\gamma}$ of the interatomic potential. $\Im_{\vec{k}(p)+\vec{k}'(p')\leftrightarrow\vec{k}''(p'')}$ can be calculated from the anharmonic interatomic force constants as

$$\Im_{\vec{k}(p)+\vec{k}'(p')\leftrightarrow\vec{k}''(p'')} = -i\left(\frac{\hbar}{2}\right)^{3/2} \sum_l \sum_{m,i} \sum_{n,j} \sum_{\alpha\beta\gamma} \left(\phi^{l(0)m(i)n(j)}_{\alpha\beta\gamma} \times \frac{e_{\alpha,l}\left(\vec{k}(p)\right) e_{\beta,m}\left(\vec{k}'(p')\right) e_{\gamma,n}\left(\vec{k}''(p'')\right)}{\sqrt{M_l M_m M_n \omega_{\vec{k}(p)}\omega_{\vec{k}'(p')}\omega_{\vec{k}''(p'')}}} \times \exp\left(i\vec{k}'\cdot\vec{R}_i\right)\exp\left(i\vec{k}''\cdot\vec{R}_j\right)\right). \quad (3)$$

Here, $\phi^{l(0)m(i)n(j)}_{\alpha\beta\gamma}$ is the anharmonic third-order interatomic force constant and depends on the total crystal energy U as

$$\phi^{l(0)m(i)n(j)}_{\alpha\beta\gamma} = -\frac{\partial^3 U}{\partial u_{\alpha,l(0)}\partial u_{\beta,m(i)}\partial u_{\gamma,n(j)}}. \quad (4)$$

The summation in Eq. (3) is overall the basis atoms l (in the reference unit cell), m (in all unit cells i), n (in all unit cells j), and overall direction indices α, β, γ spanning x, y, z, respectively. It should be noted that the summation i, j includes the reference unit cell. M_l is the mass of lth basis atom. $e_{\alpha,l}(\vec{k})$ is the component of the polarization vector of the lth basis atom in the direction α corresponding to the phonon mode $\vec{k}(p)$. Detailed derivation and subsequent simplification incorporating the symmetry of the Fourier-transformed third-order anharmonic IFC leading to the form in Eq. (3) is available in many other publications.[21,22,36] The third-order force constants depend on temperature through the lattice spacing. However, the level of anharmonicity in graphene is very low and the lattice constant changes by less than 0.2% at 650 K compared to 0 K.[37] We have checked that the anharmonic force constants are very close to the corresponding 0 K value over the temperature range investigated.

Both Normal (N) and Umklapp (U) processes are included in these computations. While N processes do not directly add thermal resistance, they create phonons with large wave vectors that facilitate U processes (which directly reverse phonon momentum and add to thermal resistance). The linearized BTE, which explicitly accounts for the dependence on nonequilibrium population of phonons undergoing N

processes, takes into account the shift of equilibrium phonon population due to N processes and does not suffer from the limitations of the relaxation time approximation.

As such, the vector equations represented by Eq. (1) form a sparse linear system for both the x and y components of the deviation function $\vec{\Psi}_{\vec{k}(p)}$, with the coefficient matrix denoted as **M.** In this work, we solve the linearized BTE for a Corbino geometry.[4,6,7] The relaxation time due to boundary scattering is $\tau_{B,\vec{k}(p)} = d/|\vec{v}_{\vec{k}(p),\alpha}|$, where d is the graphene flake diameter.

In this geometry, the boundary scattering time chosen here is more appropriate rather than $\tau_{B,\vec{k}(p)} = L/2|\vec{v}_{\vec{k}(p),\alpha}|$ (for a temperature gradient along the direction α) obtained from the Landauer formalism which is applicable for a wide graphene sheet with length L between contacts. Once the solution of the linear system specified by Eq. (1) is obtained, we can compute the 2D (in-plane) thermal conductivity tensor as

$$\kappa_{\alpha\beta} = \sum_p \int n^0_{\vec{k}(p)}\left(n^0_{\vec{k}(p)}+1\right)\frac{\hbar\omega}{k_B T}v_{\vec{k}(p),\alpha} \times \Psi_{\vec{k}(p),\beta}\frac{dk_x dk_y}{(2\pi)^2}; \quad \alpha,\beta = x,y. \tag{5}$$

A. Computational details

The numerical method described in this section is applied to calculate all possible 3-phonon scattering events in graphene and their strength (for thermal conductivity calculations). To solve the linear system of the linearized BTE [Eq. (1)], all the allowed three-phonon interaction events in graphene must be identified. Graphene Brillouin zone is discretized into elements with nk $\boldsymbol{k}$ points spaced uniformly along the wave vector magnitude and with an angular spacing of $d\theta$ degrees. The search for permissible three-phonon interactions and the computation of the matrix element for type 1 and type 2 processes need be performed only in the irreducible wedge of the graphene Brillouin zone (BZ), which corresponds to 1/12th of the full BZ. The interaction triads for all other phonon modes can be inferred by exploiting the symmetry of the Brillouin zone. In order to compute the strength of three-phonon interactions, it is critical to correctly construct the line segments of zero energy imbalance k_l for both type 1 and type 2 processes. In the present work, the line segments of interaction are accurately calculated using the following algorithm. We have found that it works well even with a coarse BZ discretization than adopted in the work.

- For a given phonon mode in the irreducible wedge, fix p' and p''.
- Sweep overall values of (k'_x, k'_y) in the entire BZ to obtain (k''_x, k''_y) using $\vec{k}+\vec{k}'+\vec{k}''=\vec{g}$. If $\vec{g}$ is non-zero, it should be noted that for a given $\vec{k}'$ and $\vec{k}''$, only one particular reciprocal vector $\vec{g}$ brings back $\vec{k}''$ into the first Brillouin zone.
- Construct the surface $\Delta\omega(k'_x, k'_y) \equiv \omega+\omega'-\omega''$ and calculate its zero contour. This results in a set of line segments k_l which may or may not be connected.

A similar algorithm is followed for processes of type 2, i.e., when a phonon decays into two different phonon modes. Figure 1 shows two such $\Delta\omega(k'_x, k'_y)$ (energy imbalance) surfaces. Figure 1(a) corresponds to the process $\mathrm{LA}(k_x=\pi/3a,\ k_y=0)+\mathrm{LA}(\vec{k}') \rightarrow \mathrm{LO}(\vec{k}'')$. Figure 1(b) corresponds to the process $\mathrm{ZA}(k_x=1.3\pi/3a,\ k_y=0)+\mathrm{ZA}(\vec{k}') \rightarrow \mathrm{TA}(\vec{k}'')$. The intersection with the plane $\Delta\omega=0$ is the corresponding k'_l contour. Using this method we obtain all the valid three-phonon interaction triads in the irreducible wedge of the graphene BZ.

The second-order (harmonic) and third-order (anharmonic) interatomic force constants for the computation of dynamical matrix and thermal conductivity are obtained by central differences of energy on a periodic graphene crystal. The harmonic and anharmonic force constants satisfy translational invariance.[38,39] We have chosen the modified Tersoff potential because we require a consistent set of second and third derivatives, the former for phonon dispersion, and the latter for thermal conductivity calculations. We also note that the parameterization obtained in Ref. 18 fits the LA/TA

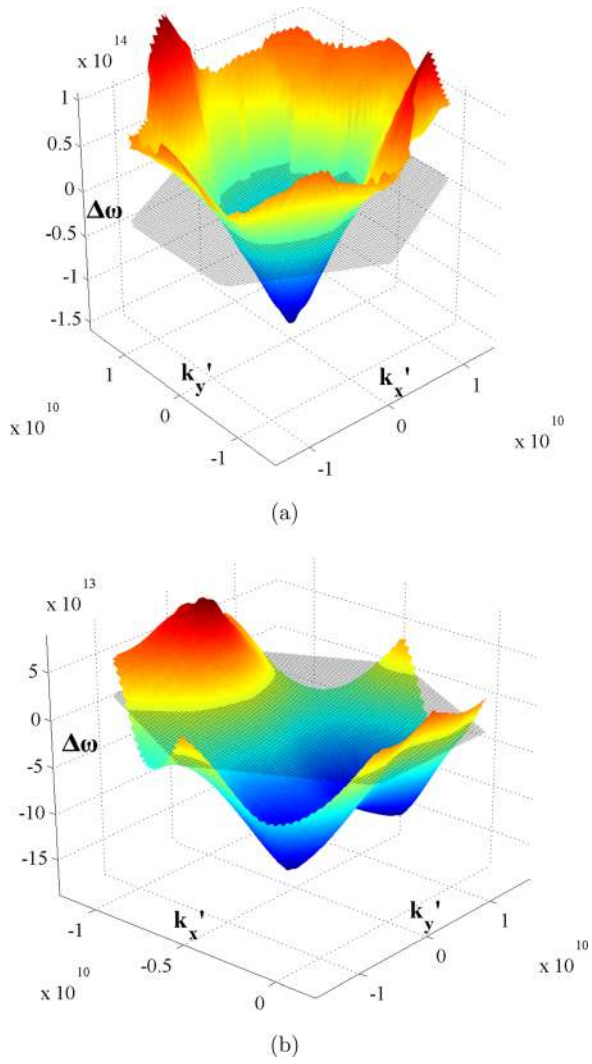

FIG. 1. (Color online) Surface of energy imbalance $\Delta\omega$ in the first BZ of graphene for the process (a) $\mathrm{LA}(k_x=\pi/3a,\ k_y=0)+\mathrm{LA}(\vec{k}') \rightarrow \mathrm{LO}(\vec{k}'')$ (b) $\mathrm{ZA}(k_x=1.3\pi/3a,\ k_y=0)+\mathrm{ZA}(\vec{k}') \rightarrow \mathrm{TA}(\vec{k}'')$.

group velocity and phonon dispersion curves (shown in[35] fairly well. The linear system of Eq. (1) is solved exactly using UMFPACK.[40,41] We also point out that an unusually fine mesh ($\sim 4500\,k$ points in the discretized Brillouin zone) is necessary for obtaining a well converged result, i.e., to capture the correct polarization wise thermal conductivity.

III. RESULTS AND DISCUSSION

A. Thermal conductivity

A discussion of phonon dispersion curves, density of states, specific heat and ballistic thermal conductance of the graphene lattice which set the stage for a general understanding of thermal transport in graphene is given in the supplementary materials.[35] The density of states exhibits the usual van Hove singularities near frequencies where the group velocity of phonon modes tends to zero.[35] Graphene exhibits a nonzero DOS even as frequency tends to zero because ZA mode exhibits quadratic dispersion. Because the ZA branch exhibits quadratic dispersion at low-to-moderate frequencies, it remains the dominant contributor to the total volumetric specific heat capacity even at room temperatures (see supplementary materials;[35] the contribution from the high frequency optical modes is negligible. The specific heat contribution and the population of ZO phonons are non-negligible and comparable to LA phonons. The high occupation of ZA phonons implies that they remain the dominant contributor to ballistic thermal conductance even at room temperature.[35] This indicates that they would also contribute to room temperature thermal conductivity even though their peak group velocity of $\sim 10^4$ m/s is lower than that of LA and TA phonons ($\sim 2 \times 10^4$ and $\sim 1.5 \times 10^4$ m/s, respectively).

1. Temperature dependence

Figure 2 shows the variation of diffusive thermal conductivity ($\tau_B \rightarrow \infty$) with temperature of the graphene sheet (along with the contribution of each polarization) along the $\Gamma - M$ direction. At room temperature the net contribution by each polarization (in W/m K) is ZA: 2859, TA: 242, LA: 91.5, ZO: 23. The contribution by ZA phonons far exceeds that due to LA and TA phonons. However, it is worth noting that the contribution of LA, TA phonons is still quite high ($\sim$335) compared to most other crystalline materials such as Si and Ge. This result derives from the high specific heat capacity and moderately high group velocity of ZA phonons but more importantly from the anharmonic selection rule that arises out of the reflection symmetry of the graphene layer. As noted by Seol *et al.*,[8] this implies that any third derivative of the potential of the form $\phi_{z\beta\gamma}^{l(0)m(i)n(j)}$; $\alpha, \beta = x, y$ and $\phi_{zzz}^{l(0)m(i)n(j)}$ or any other permutation of these is zero. Since the eigenvectors of the in-plane modes are completely decoupled from the flexural modes, this means that three-phonon scattering processes involving any out-of-plane phonons (such as ZA and ZO) must have an even number of these out-of-plane phonons. Details about this selection rule have been discussed by Lindsay *et al.*[24] This potentially eliminates a large number of possible three-phonon scattering processes that satisfy energy and momentum conservation and would be legitimate three-phonon scattering processes. The theoretically obtained variation of graphene thermal conductivity with temperature is also compared against the experimental measurements reported in Chen *et al.*[7] for a wide range of graphene flake lengths, ranging from 2.9–10 μm. The comparison between the two is remarkably close over the entire temperature range without the use of fitting parameters and validates the theory presented here. A similar set of calculations have also been performed to calculate thermal conductivity of few-layer graphene.[42] The evolution from single layer graphene to bulk graphite with increasing number of layers was found to be due to reduced contribution from flexural phonons.

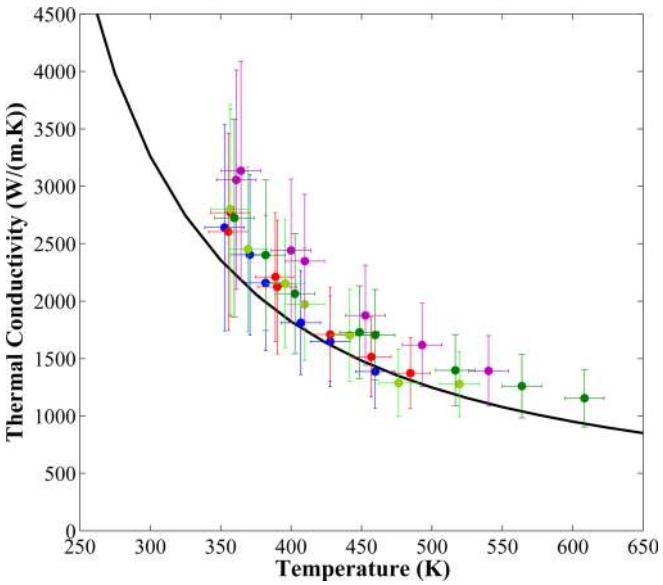

FIG. 2. (Color online) Diffusive thermal conductivity variation of graphene sheet with temperature along the $\Gamma - M$ direction and comparison with the experimental data of Chen *et al.*[7]

Our calculations show that finite graphene sheet diameter can lead to lower thermal conductivity due to boundary scattering of phonons. However, significant size effects on thermal conductivity are seen only below a few microns. It is observed that the diffusive thermal conductivity values presented here (which do not include the effect of boundary scattering) are obtained for graphene sheet diameter, $d > 10\,\mu$m. Furthermore, it is the component of thermal conductivity from flexural phonons that exhibits the strongest dependence on diameter.[35] These results are in broad agreement with the trends reported in.[24] This may also explain why no clear size dependence was seen in the measured thermal conductivity of graphene flakes with diameter ranging from 3–10 μm[7] which was earlier attributed to scattering from grain boundaries and wrinkles in the graphene sheet on the scale of 5–20 μm. More details of the dependence of polarization wise and total thermal conductivity on temperature, T and sheet diameter, d can be found in the supplementary materials.[35]

2. Phonon population and frequency dependence

At room temperature, the diffusive thermal conductivity calculated from a numerical solution of the linearized BTE is 3260 W/mK, and is more than 3 times higher than the corresponding value obtained from the single mode relaxation

time approximation (SMRT). At higher temperatures, as the strength of anharmonic scattering increases, this factor decreases to ~2. The observed difference between the SMRT and the computed thermal conductivity is much larger than seen in 3D crystals such as Si, Ge[21,39] but commensurate with those of CNTs.[43] In this section, we consider the particularly unintuitive behavior of phonon population that leads to high thermal conductivity of graphene and renders the SMRT approximation inaccurate in modeling its thermal conductivity. Figure 3 plots $\vec{\Psi}_{\vec{k}(p)}$ and $\vec{\Psi}^0_{\vec{k}(p)}$ (the corresponding value under the SMRT) for the acoustic phonon polarizations along the $\Gamma - M$ direction ($+x$). Under the SMRT, the sign of $\vec{\Psi}^0_{\vec{k}(p)}$ for a given phonon mode is determined by the sign of its corresponding velocity component. LA, ZA, and TA phonons therefore have a positive value. The exact value of the deviation function increases in magnitude for the most part, with a large increase for ZA modes. ZA phonons along the $\Gamma - M$ direction (also denoted here as the $+x$ axis) interact with many other ZA phonons through scattering of types ZA + ZA → LA and ZA + ZA → TA (shown in the supplementary materials.[35] These type 1 processes contribute a positive value in the sum [Eq. (1)], so that in the high wave vector region, values of $\vec{\Psi}_{\vec{k}(p)}$ for LA (and also for TA) phonons ultimately become negative (through the reverse LA → ZA + ZA and LA → LA + LA processes). The net effect is the creation of a small region in frequency space (in the current paper, all the reported frequencies should be read as angular frequencies; 1 Hz = 1 rad/s) where LA phonons carry heat in the direction of the applied temperature gradient. Clearly, this negative shift will be most prominent for phonons in the $\Gamma - M$ direction (due to high v_x). We emphasize that these processes make thermal transport in graphene quite unique and render the SMRT approximation invalid as the deviation of each phonon mode strongly depends on the deviation of the other phonon modes with which it undergoes anharmonic scattering. Figure 4 plots the polarization-specific cumulative diffusive thermal conductivity variation with frequency at 300 and 500 K. It should be noted that thermal conductivity contribution from all acoustic modes spreads across the entire Brillouin zone or the frequency range corresponding to each polarization (the corresponding maximum/cutoff frequency for each acoustic branch is also labeled in Fig. 4). Particularly for ZA modes, the frequency dependence shown in Fig. 4 implies that most thermal energy is carried by moderate-to-large wave vectors since low wave vector phonons have very low frequency and group velocity. This result contrasts with a common assumption in phonon modeling[12,13,15,16] that higher three-phonon scattering rates are more than offset by lower phonon populations toward the edges of the Brillouin zone. It should be noted here that TA and LA phonons contribute a "negative" component to the net thermal conductivity in the high frequency range, resulting in wiggles in the cumulative thermal conductivity for TA and LA contributions in Fig. 4. This negative contribution is absent under the SMRT approximation because the phonon distribution of each mode is shifted against the direction of temperature gradient; thereby the cumulative thermal conductivity always shows a monotonic increase with frequency. However, in the solution of Eq. (1), where the population deviation of each phonon mode $\vec{\Psi}_{\vec{k}(p)}$ depends on the $\vec{\Psi}$ vector of all other phonons modes that $\vec{k}(p)$ interacts with, a negative contribution to thermal conductivity from some phonon groups may result; this is especially true as the strength of anharmonic scattering increases. For example, along the $\Gamma - M$ direction, there exist a sufficient number of LA → ZA + ZA (and TA → ZA + ZA) processes (mostly U and some N) that generate ZA phonons with momentum opposite to the LA (or TA) phonon and contribute to this effect. This is only true for the high wave vector LA/TA phonons with a sufficient number of such U processes; indirectly these are the very processes that lead to a relatively higher contribution by ZA modes.

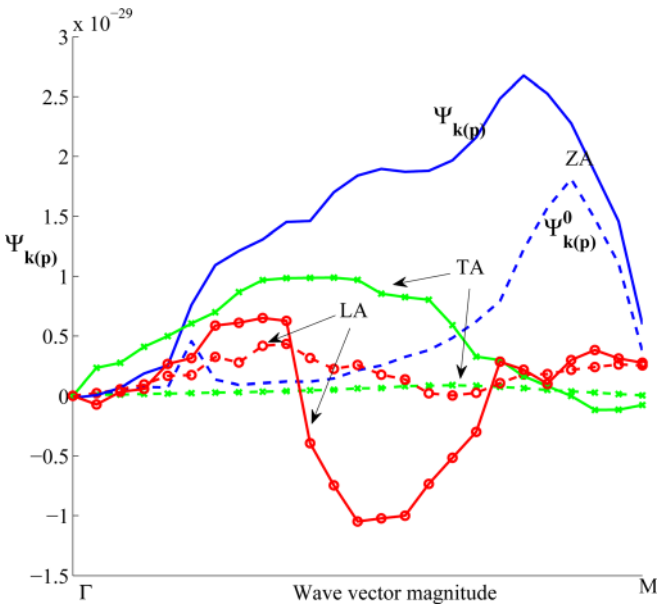

FIG. 3. (Color online) Plot of the function $\vec{\Psi}_{\vec{k}(p)}$ (solid lines) and $\vec{\Psi}^0_{\vec{k}(p)}$ (dashed lines) at T = 300 K.

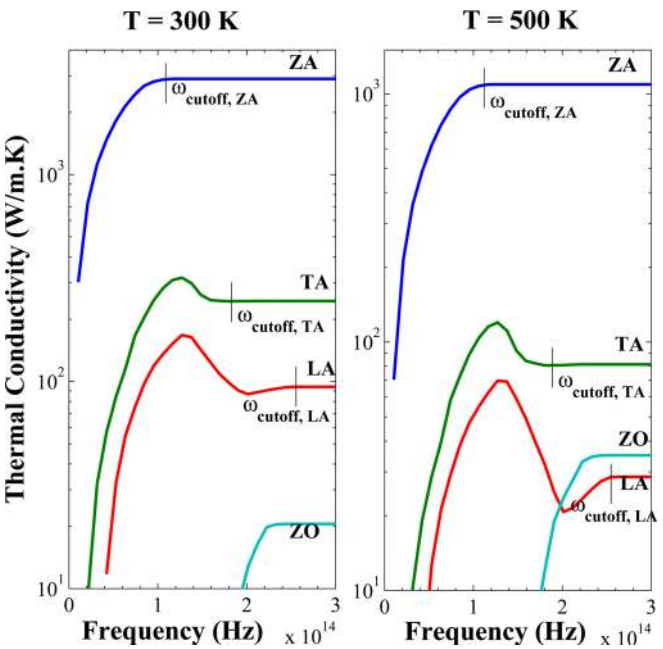

FIG. 4. (Color online) Cumulative thermal conductivity contributions by each phonon branch vs frequency at 300 and 500 K.

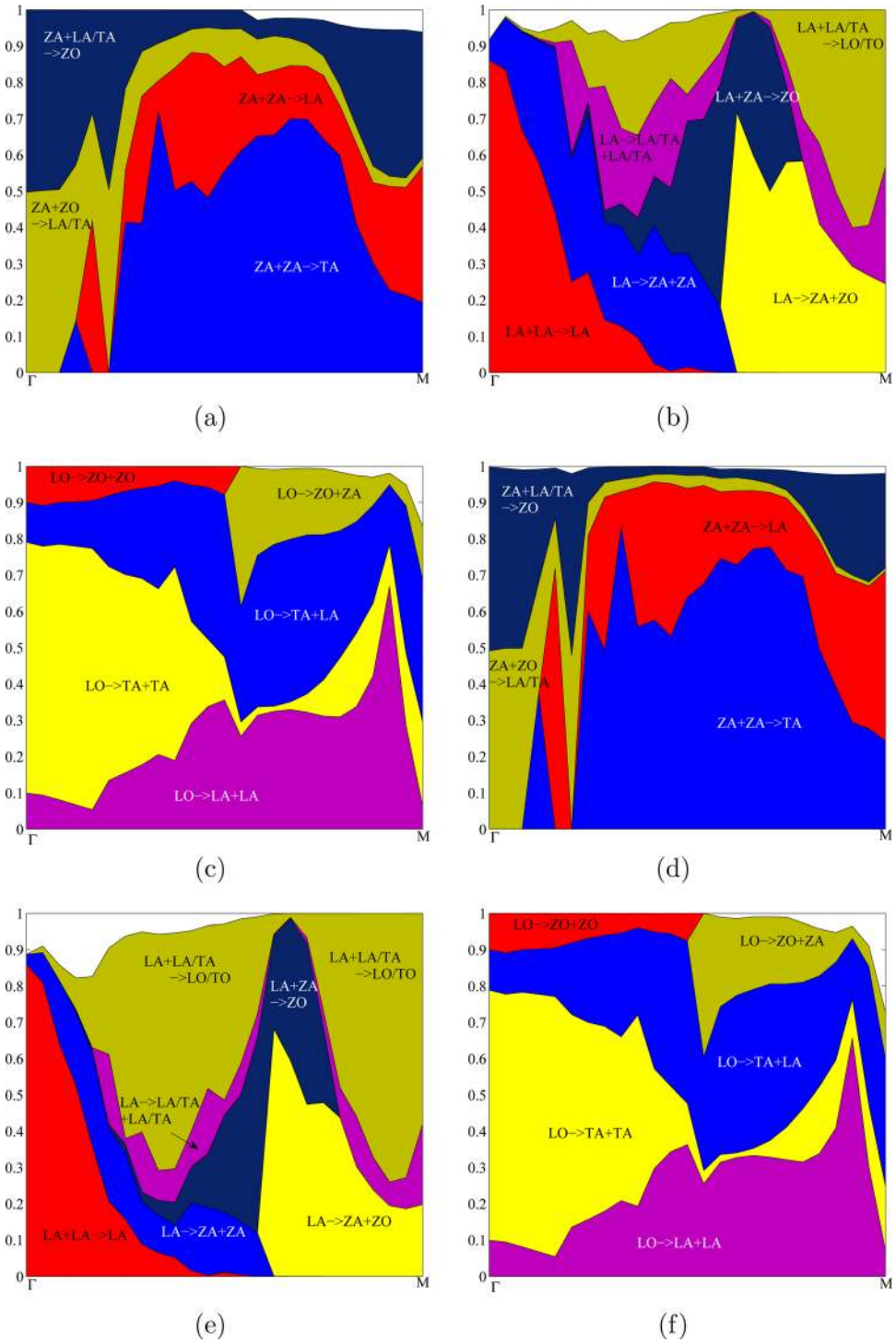

FIG. 5. (Color online) Relative contribution to $\Gamma_{\vec{k}(p)}$ of different three-phonon scattering channels for ZA, LA, and LO phonons against the phonon wave vector magnitude along the $\Gamma - M$ direction. (a)–(c) correspond to 300 K while (d)–(f) correspond to 800 K.

B. Selection rules, scattering channels, and their relative importance

In this section, we explore the physical mechanisms that lead to thermal conductivity variations seen in the previous section. Of particular importance is the scattering detail of ZA phonons that lends graphene its extremely high thermal conductivity. We also present in detail the scattering mechanisms associated with the longitudinal phonons which are of prime importance in understanding electro-thermal transport. This is because electron-phonon N scattering processes generate phonons which have a polarization vector aligned with the phonon wave vector, a condition satisfied only by longitudinal phonons.[34] This makes the efficiency of energy transfer from LA/LO phonons to ZA phonons an important factor in determining whether or not the high thermal conductivity of graphene (which is due mostly to ZA phonons) may be successfully exploited in electronic devices for heat dissipation. $\Gamma_{\vec{k}(p)}$ [Eq. (2)] collectively quantifies all scattering mechanisms, accounting for their relative importance based on:

1. The magnitude of the matrix element for three-phonon scattering (which ties it to crystal anharmonicity);

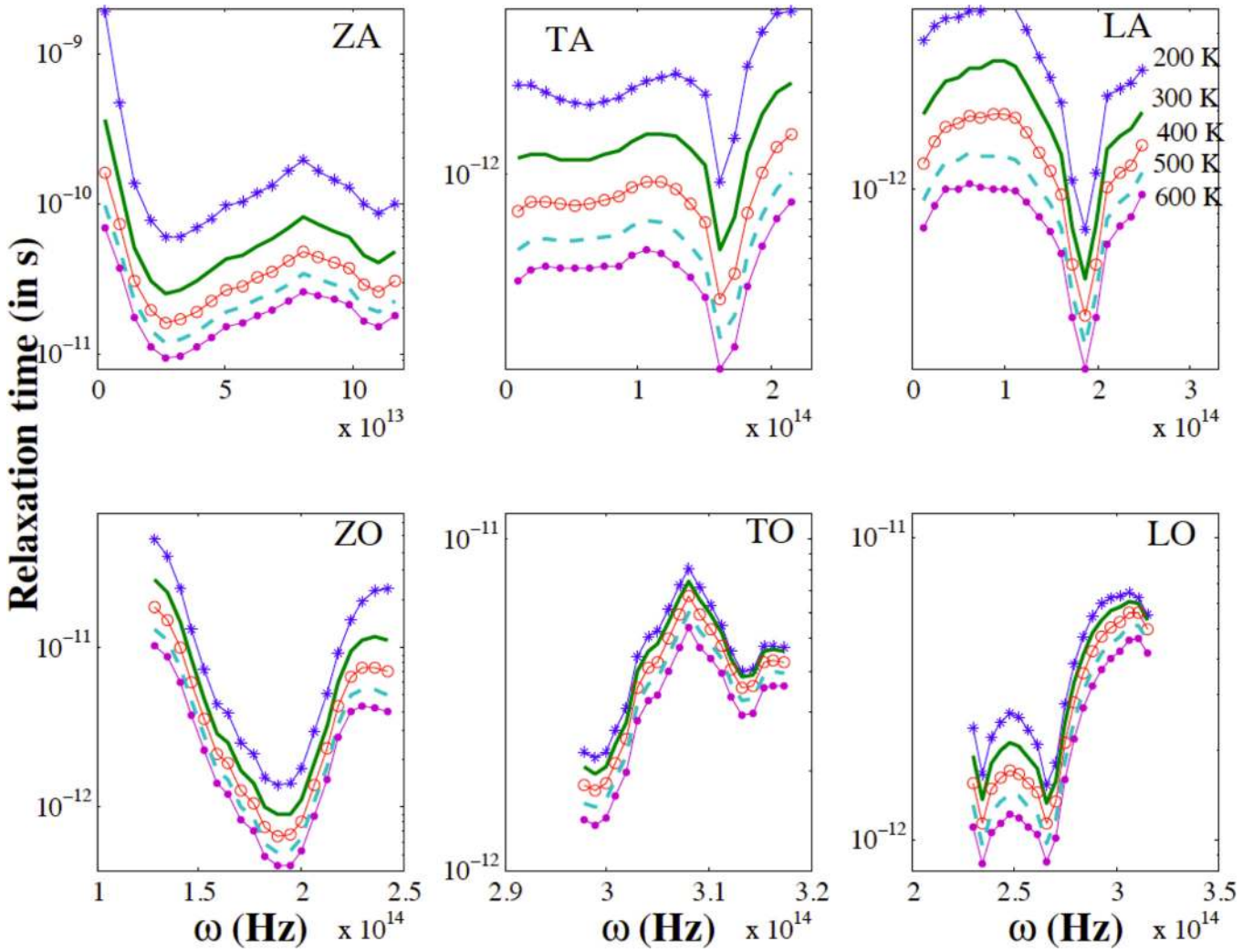

FIG. 6. (Color online) Relaxation time of various phonon polarizations vs phonon frequency from 200–600 K. Frequency range and the limits on relaxation time are different for each polarization.

2. occupation number of different phonon modes involved in the scattering processes (through the dependence on $n^0_{\vec{k}(p)}$, $n^0_{\vec{k}'(p')}$ and $n^0_{\vec{k}''(p'')}$; and
3. the joint density of states (the available number of phonon pairs $\vec{k}'(p')$ and $\vec{k}''(p'')$ for the scattering processes) through integration along the contour of zero energy imbalance k'_l and the normal velocity component v'_n.

Though it does not take into account the deviation from equilibrium of the phonon occupation, $\Gamma_{\vec{k}(p)}$ serves as an important measure of the relative importance of various scattering channels (as it is a simple sum overall different pathways). Figure 5 shows the relative contribution of each three-phonon scattering pathway to $\Gamma_{\vec{k}(p)}$ for ZA (a), (d); LA (b), (e), and LO (c), (f) phonon modes respectively against their wave vector at 300 K [(a)–(c)] and 800 K [(d)–(f)]. The contributions should sum to unity; where they do not, the deficit corresponds to contribution by boundary scattering or a few other pathways that are not significant.

It is seen that the primary anharmonic scattering of ZA phonons occurs through the ZA + ZA → LA or ZA + ZA → TA channels throughout most of the BZ. As pointed out earlier, any other mechanisms involving an odd number of out-of-plane polarized phonons are suppressed as the corresponding third-derivatives of the potential are zero. Also, due to the low frequency range of ZA phonons, processes of type 2 do not play a significant role. The trend is similar at 800 K except that the share of scattering by optical modes increases due to their increased occupation. For LA phonons, there is a variety of combinations that become active depending on the wavevector region. Figure 5(b) and Fig. 5(e) show that the important scattering mechanisms are type 2, i.e., LA → ZA + ZA, LA → ZA + ZO, and LA → LA/TA + LA/TA throughout most of the BZ. This means that a strong component of anharmonic scattering for LA phonons involves the generation of ZA phonon modes. At higher temperatures, the acoustic-acoustic-optical (*aao*) scattering pathway dominates; this is common in other materials as well, for example, in Si and CNTs. At low wave vectors, the N processes LA + LA → LA are also particularly strong.

Finally, the decay of LO phonons is mainly through the LO → LA/TA + LA/TA type 2 process. The high frequency range of these phonon modes inhibits most type 1 processes. In the midhigh wave vector regime, the creation of ZA phonons through the LO → ZA + ZO channel is also active. However, it contributes in a rather small proportion. This

means that most of the energy input into LO phonon modes would not be received by ZA phonons directly, with a strong possibility creating a phonon-phonon decay bottleneck.

C. Phonon relaxation times

The single mode relaxation time (SMRT) of a given phonon mode may be written as

$$\tau^{\text{smrt}}_{\vec{k}(p)} = \frac{n^0_{\vec{k}(p)}\left(n^0_{\vec{k}(p)}+1\right)}{\Gamma_{\vec{k}(p)}}. \quad (6)$$

Although the single mode relaxation time approximation is inadequate for computing the thermal conductivity of graphene, phonon relaxation times can be used to provide an estimate of the scattering rate, especially at high temperatures. From the single mode relaxation time, frequency-dependent relaxation time for each frequency is obtained as

$$\tau_{\omega,p} = \frac{\int \tau^{\text{smrt}}_{\vec{k}(p)}\delta(\omega-\omega_{\vec{k}(p)})dk_x dk_y}{\int \delta(\omega-\omega_{\vec{k}(p)})dk_x dk_y}. \quad (7)$$

This expression averages the relaxation time with the corresponding density of states overall different phonon modes of a certain polarization in the crystal.

Figure 6 shows the dependence of the single mode relaxation time for phonons of each polarization versus the phonon frequency. The temperature range considered here is 200–600 K. The following observations can be made from the plots of relaxation time versus frequency:

- A monotonic decrease of relaxation time with increase in frequency, such as that predicted by typical long wavelength approximations of the matrix elements and classical approximations of the phonon distribution in[12,13,15,16] is not observed in the case of graphene. The reason is a combination of high frequencies involved in the phonon dispersion coupled with the peculiar selection rules for three-phonon scattering.
- Over the temperature range considered (200–600 K), relaxation times for all ZA, LA, and TA phonon groups decrease by an order of magnitude. The ZA phonon relaxation time is seen to increase with frequency in the low frequency region.
- Overall, at 300 K, the relaxation time of ZA phonons is approximately 50–200 ps. ZO phonons exhibit a strong dependence on frequency, with the relaxation time spanning 1–50 ps. Most other phonon modes, on the other hand, show a relaxation time in a narrow range of 1–10 ps. This comparable to the high frequency LA/TA phonon relaxation time in materials such as silicon.

In addition, we assess the characteristic relaxation time for scattering processes in which ZA phonon generation takes place due to anharmonic scattering with LA or LO modes (including type 1 and type 2), owing to their particular importance in thermal transport. Figure 7 plots this characteristic relaxation time between LA-ZA modes. This is

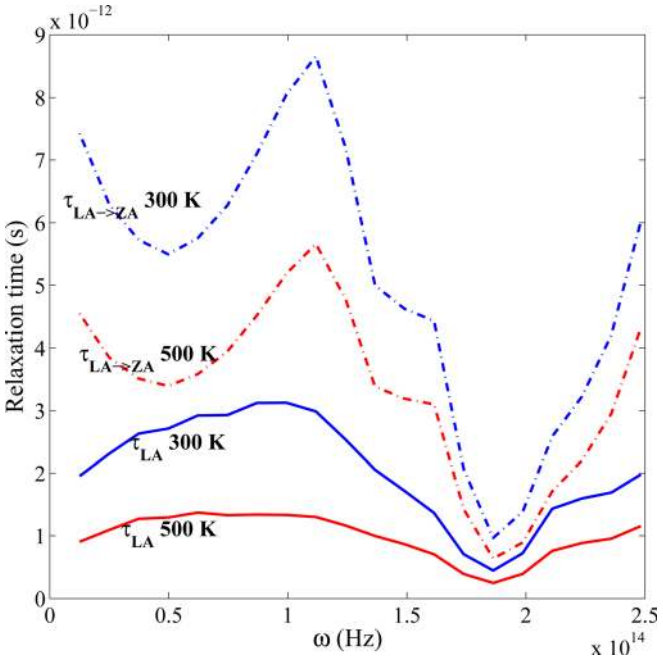

FIG. 7. (Color online) Characteristic time scale for LA → ZA energy exchange along with the LA phonon relaxation time.

estimated by a selective summation in Eq. (2) over three-phonon scattering events that involve generation of a ZA phonon. Also plotted is the net relaxation time of LA phonons. At 300 K this LA-ZA relaxation time is about 5–15 ps and is 3–4 times higher than the net relaxation time of LA phonons. This difference is more pronounced as temperature increases because the relative strength of other scattering mechanisms for LA modes dominates over the LA→ZA conversion (at higher temperatures, occupation of high frequency acoustic and optical modes increases the scattering to these modes). The implication of this time is that exchange of energy from LA to ZA phonons takes place over a length scale ~200 nm at room temperature (using v_{LA} ~20,000 m/s). Suspended graphene electronics operating on these length scales will therefore suffer from a bottleneck to thermal transport.[44,45] The same trend calculated for LO phonons shows that the LO-ZA energy exchange time scale is orders of magnitude higher than the relaxation time of LO phonons which means that energy exchange from LO → ZA phonons will most likely occur indirectly through processes such as LO→LA→ZA and LO→TA→ZA.

These processes are also important in thermal conductivity measurements using laser heating of graphene sheets.[3,4,6] Our computations indicate that the LA→ZA scattering rate is about an order of magnitude smaller than the rate at which electron-phonon energy exchange takes place. Therefore, a bottleneck would be encountered in the energy transfer from the longitudinal to the ZA modes. The effect is exacerbated for larger laser spot sizes (for the same sample size) because there would insufficient residence time for the LA→ZA process to occur. Furthermore, we expect a high level of non-equilibrium between phonon groups due to this difference in the time scales of energy generation and dissipation. Consequently, near-equilibrium approaches, based

for example on Fourier conduction, would yield erroneous estimates of thermal conductivity if used to post-process measurements. More importantly, recent measurements have shown a clear dependence of measured thermal conductivity on the laser spot size.[3,4,6] Local nonequilibrium between LA/LO and ZA modes in the heated region would ascribe a higher value to the measured temperature (from Raman spectroscopy) than the true lattice temperature, which is a weighted average overall phonon modes. Because the measured thermal conductivity is inversely proportional to the temperature difference between the center and the contacts, the measured thermal conductivity should decrease with increasing laser spot sizes (due to the increased region of nonequilibrium). Also, this non-equilibrium will be less severe at higher temperatures since the energy transfer between LA and ZA phonons becomes more efficient due to increased anharmonic scattering. This trend is clearly evident in the measurements reported by Cai *et al.*[4] with the laser spot radius of 170 and 280 nm. As inferred from the data, at temperatures around 350 K, the measured difference in thermal conductivity is greater than 25% (with a higher value at lower laser spot radius) but this difference quickly diminishes as temperature increases. The thermal conductivity of graphene measured by Faugeras *et al.*[6] is 630 W/m K with a laser spot radius of $\sim 1\ \mu$m and is significantly lower than those for graphite and for single layer graphene in Cai *et al.*[4] at the same temperature. We again ascribe this discrepancy to the large laser spot radius. However, the measurements reported by Balandin *et al.*[3] are higher than those reported by Cai *et al.*[4] even though larger laser spot sizes were used, but this result may derive from an overestimate of the absorbed laser power in the former set of experiments.

D. Comparison with literature

Our total thermal conductivity predictions agree reasonably well with those reported by Lindsay *et al.*[24] using the same theory and parameters to analyze thermal conductivity in graphene. The general conclusion about selection rules for ZA/ZO phonons, and the frequency and temperature dependence of thermal conductivity is similar to Lindsay *et al.*;[24] our results also indicate that ZA phonons contribute significantly to thermal transport. However, we find a significantly lower contribution by LA/TA phonons and a higher contribution by ZA phonons. Nika *et al.*,[12] also analyzed thermal conductivity under the relaxation time and long-wavelength approximations, and accounted for Umklapp scattering processes only. The computational method presented here is very similar to theirs, and with the use of the Klemens matrix element,[14] we compute thermal conductivity values which are in a good agreement with Nika *et al.*[12] Their simulations show much stronger size dependence (as N processes are not accounted for) and attribute thermal conductivity mainly to LA and TA phonons, in contrast to what is observed by us in the present work. Our computation shows that the behavior observed by Nika *et al.*[12] arises mainly from the long wavelength approximation. Numerous molecular dynamics simulations of graphene and graphene nanoribbons have been performed by various groups[30–33] and have been reported thermal conductivity in the range 400–10000 W/m K. It is noteworthy that while most MD simulations using the REBO/Brenner potential have reported a diffusive thermal conductivity of graphene in the range 400–700 W/m K, the use of Tersoff potential with the original parameterization[17] has shown a much higher thermal conductivity, in the range $\sim$8000–12000 W/m K.[33] The use of the original parameter set in analyzing room temperature thermal conductivity using the solution of linearized BTE has shown a lower thermal conductivity compared to a previous report[18] and our simulations in this paper, which uses the modified parameterization of Lindsay and Broido.[18] A direct comparison with these studies is difficult as the potential parameters are not the same, and none of the published MD studies have given a complete mode-wise detail of phonon transport in graphene. Some of these discrepancies may arise from the classical nature of MD simulations which may entail significant errors for carbon at room temperature.

IV. CONCLUSIONS

In this work, a framework for the computation of phonon dispersion and three-phonon scattering events is developed and applied to calculate the intrinsic phonon scattering processes in graphene. Subsequently, single-mode relaxation time and thermal conductivity values for graphene are presented. The results reveal a detailed mode-wise picture of thermal conductivity in graphene, demonstrating which phonons dominate heat conduction in graphene and those that would suffer the effect of boundary scattering the most. The detailed dependence of relaxation time on frequency and temperature is presented to enable estimation of temperature distributions and phonon decay channels. This information is necessary for accurate characterization of electrothermal transport and Joule heating in graphene-based electronics and interconnects and in interpreting thermal conductivity experiments based on Raman spectroscopy. The procedure outlined above has also been used to calculate phonon scattering mechanisms in few-layer graphene.

ACKNOWLEDGMENTS

This material is based upon work partially supported by the Defense Advanced Research Projects Agency and SPAWAR Systems Center, Pacific under Contract No. N66001-09-C-2013. The authors would like to thank the research groups of Professor Li Shi and Rodney Ruoff for kindly providing the experimental data on thermal conductivity of graphene. We also acknowledge useful discussions with Lucas Lindsay and Jose A. Pascual Gutierrez.

[1]E. Pop, D. Mann, J. Cao, Q. Wang, K. Goodson, and H. Dai, Phys. Rev. Lett. **95**, 155505 (2005).
[2]P. Kim, L. Shi, A. Majumdar, and P. L. McEuen, Phys. Rev. Lett. **87**, 215502 (2001).
[3]A. A. Balandin, S. Ghosh, W. Bao, I. Calizo, D. Teweldebrhan, F. Miao, and C. N. Lau, Nano Lett. **8**, 902 (2008).
[4]W. Cai, A. L. Moore, Y. Zhu, X. Li, S. Chen, L. Shi, and R. S. Ruoff, Nano Lett. **10**, 1645 (2010).
[5]S. Ghosh, W. Bao, D. L. Nika, S. Subrina, E. P. Pokatilov, C. N. Lau, and A. A. Balandin, Nat. Mater. **9**, 555 (2010).

[6]C. Faugeras, B. Faugeras, M. Orlita, M. Potemski, R. R. Nair, and A. K. Geim, ACS Nano **4**, 1889 (2010).
[7]S. Chen, A. L. Moore, W. Cai, J. W. Suk, J. An, C. Mishra, C. Amos, C. W. Magnuson, J. Kang, L. Shi, and R. S. Ruoff, ACS Nano **5**, 321 (2010).
[8]J. H. Seol, I. Jo, A. L. Moore, L. Lindsay, Z. H. Aitken, M. T. Pettes, X. Li, Z. Yao, R. Huang, D. Broido, N. Mingo, R. S. Ruoff, and L. Shi, Science **328**, 213 (2010).
[9]Z. Wang, R. Xie, C. T. Bui, D. Liu, X. Ni, B. Li, and J. T. L. Thong, Nano Lett. **11**, 113 (2010).
[10]W. Jang, Z. Chen, W. Bao, C. N. Lau, and C. Dames, Nano Lett. **10**, 3909 (2010).
[11]J. M. Dawlaty, S. Shivaraman, M. Chandrashekhar, F. Rana, and M. G. Spencer, Appl. Phys. Lett. **92**, 042116 (2008).
[12]D. L. Nika, E. P. Pokatilov, A. S. Askerov, and A. A. Balandin, Phys. Rev. B **79**, 155413 (2009).
[13]B. D. Kong, S. Paul, M. B. Nardelli, and K. W. Kim, Phys. Rev. B **80**, 033406 (2009).
[14]F. Seitz and D. Turnbull, *Solid State Physics* (Academic, New York, 1958).
[15]P. G. Klemens, J. Wide Bandgap Mater. **7**, 332 (2000).
[16]P. G. Klemens and D. F. Pedraza, Carbon **32**, 735 (1994).
[17]J. Tersoff, Phys. Rev. Lett. **61**, 2879 (1988).
[18]L. Lindsay and D. A. Broido, Phys. Rev. B **81**, 205441 (2010).
[19]M. Omini and A. Sparavigna, Phys. Rev. B **53**, 9064 (1996).
[20]D. A. Broido, M. Malorny, G. Birner, N. Mingo, and D. A. Stewart, Appl. Phys. Lett. **91**, 231922 (2007).
[21]J. A. Pascual-Gutierrez, J. Y. Murthy, and R. Viskanta, J. Appl. Phys. **106**, 063532 (2009).
[22]G. P. Srivastava, *The Physics of Phonons* (Hilger, Bristol, Philadelphia, 1990).
[23]A. Chernatynskiy and S. R. Phillpot, Phys. Rev. B **82**, 134301 (2010).
[24]L. Lindsay, D. A. Broido, and N. Mingo, Phys. Rev. B **82**, 115427 (2010).
[25]J. R. Lukes and H. Zhong, J. Heat Transfer **129**, 705 (2007).
[26]D. Donadio and G. Galli, Phys. Rev. Lett. **99**, 255502 (2007).
[27]A. V. Savin, B. Hu, and Y. S. Kivshar, Phys. Rev. B **80**, 195423 (2009).
[28]J. A. Thomas, R. M. Iutzi, and A. J. H. McGaughey, Phys. Rev. B **81**, 045413 (2010).
[29]J. Shiomi and S. Maruyama, Phys. Rev. B **73**, 205420 (2006).
[30]J. Hu, X. Ruan, and Y. P. Chen, Nano Lett. **9**, 2730 (2009).
[31]Z. Guo, D. Zhang, and X.-G. Gong, Appl. Phys. Lett. **95**, 163103 (2009).
[32]J. Hu, S. Schiffli, A. Vallabhaneni, X. Ruan, and Y. P. Chen, Appl. Phys. Lett. **97**, 133107 (2010).
[33]W. J. Evans, L. Hu, and P. Keblinski, Appl. Phys. Lett. **96**, 203112 (2010).
[34]J. Ziman, *Electrons and Phonons* (Oxford University Press, Oxford, 2000).
[35]See supplementary materials at http://dx.doi.org/10.1063/1.3656451 for the description of phonon dispersion, ballistic thermal conductance, linearized BTE and size dependence of thermal conductivity in single layer graphene.
[36]A. Ward, "First principles of the lattice thermal conductivity of semiconductors," Ph.D. thesis, (Boston College, 2009).
[37]N. Mounet and N. Marzari, Phys. Rev. B **71**, 205214 (2005).
[38]A. A. Maradudin, *Theory of Lattice Dynamics in the Harmonic Approximation* (Academic, New York, 1971).
[39]D. A. Broido, A. Ward, and N. Mingo, Phys. Rev. B **72**, 014308 (2005).
[40]T. A. Davis, ACM Trans. Math. Softw. **30**, 165 (2004).
[41]T. A. Davis, ACM Trans. Math. Softw. **30**, 196 (2004).
[42]D. Singh, J. Y. Murthy, and T. S. Fisher, J. Appl. Phys. **110**, 044317 (2011).
[43]L. Lindsay, D. A. Broido, and N. Mingo, Phys. Rev. B, **80**, 125407 (2009).
[44]D.-H. Chae, B. Krauss, K. von Klitzing, and J. H. Smet, Nano Lett. **10**, 466 (2009).
[45]I. Jo, I.-K. Hsu, Y. J. Lee, M. M. Sadeghi, S. Kim, S. Cronin, E. Tutuc, S. K. Banerjee, Z. Yao, and L. Shi, Nano Lett. **11**, 85 (2010).